Fuel 185 (2016) 243–253

Contents lists available at ScienceDirect

Fuel

journal homepage: www.elsevier.com/locate/fuel

Full Length Article

Extension of PREMIER combustion operation range using split micro pilot fuel injection in a dual fuel natural gas compression ignition engine: A performance-based and visual investigation

Cagdas Aksu [a,*], Nobuyuki Kawahara [b], Kazuya Tsuboi Assistant Professor [c], Morio Kondo [d], Eiji Tomita Professor [b]

[a] Heat Power Engineering Laboratory, Division of Industrial Innovation Sciences, Graduate School of Natural Science and Technology, Okayama University, Tsushima-Naka 3-1-1, Kita-Ku, Okayama 700-8530, Japan
[b] Heat Power Engineering Laboratory, Department of Energy Systems Engineering, Division of Industrial Innovation Sciences, Graduate School of Natural Science and Technology, Okayama University, Tsushima-Naka 3-1-1, Kita-Ku, Okayama 700-8530, Japan
[c] Department of Advanced Mechanics, Division of Industrial Innovation Sciences, Graduate School of Natural Science and Technology, Okayama University, 3-1-1 Tsushima-naka, Kita-ku, Okayama 700-8530, Japan
[d] Machinery Factory Technology Support & Development Department, Mitsui Engineering & Shipbuilding Co., Ltd. Tamano Works, 1-1, Tama 3-chome, Tamano, Okayama 706-8651, Japan

HIGHLIGHTS

- Split injection can suppress knocking to PREMIER combustion.
- Split injection can promote normal combustion to PREMIER combustion.
- Maximum of usable thermal efficiency is extended by suppressing knocking.
- Flame kernel size and rate of growth changes the combustion mode.
- Flame kernel properties are affected by timing of second injection.

ARTICLE INFO

Article history:
Received 13 April 2016
Received in revised form 6 July 2016
Accepted 29 July 2016
Available online 4 August 2016

Keywords:
Dual fuel combustion
PREMIER combustion
Micro pilot fuel injection
Split injection
Visualization
Natural gas

ABSTRACT

The effects of split pilot fuel injection on engine performance and PREmixed Mixture Ignition in the End Gas Region (PREMIER) combustion characteristics were investigated in a single-cylinder dual-fuel natural gas engine ignited with diesel fuel. In particular, the effect of second spray timing on combustion mode was examined. PREMIER combustion was observed in a wider range of operating conditions with split injection strategy compared to single injection strategy. We determined that it was possible to both decelerate heat release and suppress knocking to PREMIER combustion, and accelerate heat release and promote normal combustion to PREMIER combustion, with suitable second injection timing. The maximum of thermal efficiency of PREMIER combustion operation with split injection was close to the results obtained with knocking operation. In-cylinder images showed that split injection strategy advances or retards the progress of combustion by controlling the size and rate of growth of flame kernels, depending on the timing of the second injection. The combustion progress is earlier when the pilot fuel delivered during the first injection autoignites during the second injection. Kernel growth and the final size were adversely affected when the second injection was initiated after pilot fuel autoignition.

1. Introduction

The use of petroleum as an energy source is becoming less feasible due to the depletion of global oil reserves, its negative impact on the environment, and strict exhaust emission norms. This situation affects compression ignition (CI) engines in particular because of their role in transportation and electricity generation

* Corresponding author.
E-mail addresses: cagdasaksu@gmail.com (C. Aksu), kawahara@okayama-u.ac.jp (N. Kawahara), tsuboi@okayama-u.ac.jp (K. Tsuboi), mkondo@mes.co.jp (M. Kondo), etomita@okayama-u.ac.jp (E. Tomita).
URLs: https://powerlab.mech.okayama-u.ac.jp/ (N. Kawahara), https://powerlab.mech.okayama-u.ac.jp/ (K. Tsuboi), https://powerlab.mech.okayama-u.ac.jp/ (E. Tomita).

http://dx.doi.org/10.1016/j.fuel.2016.07.120
0016-2361/

industries, emphasizing on the need for cleaner, more economical and reliable alternatives. Alternative fuels can solve these issues without significant compromise [1–4]. Natural gas is one such fuel, due to its abundance and clean combustion properties.

Natural gas is a mixture of mainly methane as the primary combustible gas, with traces of hydrocarbon gases and diluents, the fractions of which depend on the region of extraction and purification processes. Due to its methane-rich composition, natural gas is a clean-burning fuel and is globally becoming a more popular fuel source. Natural gas constituted 14% of total final consumption of world energy sources in 1973, which increased to 15.1% in 2013; the fraction used for transportation increased from 2.7% to 6.9% over this 40-year interval [5].

Use of natural gas in spark ignition (SI) engines and CI engines has been researched extensively. Especially, its use in dual-fuel CI has attracted much attention due to the high efficiency of such engines. Dual-fuel CI engines are suitable platforms for using gaseous fuels with high autoignition temperatures, one of which is natural gas. In this combustion mode, an air-gaseous fuel mixture is ignited by the pilot fuel. By its nature, autoignition of the pilot fuel creates a large zone of flames, the flame kernel. A profound improvement over SI, the CI configuration eliminates smoke emission and enables lean operation by reducing the risk of misfiring; however, increased unburned hydrocarbon (HC) and carbon monoxide (CO) emissions remain an issue [6,7]. Fundamental knowledge on the combustion of many gaseous fuel types, including natural gas, under dual-fuel operation conditions has been presented by Karim et al. [6–9]. These works report that the dual fuel operation range is limited by knocking at the higher load end and by misfiring at the lower load end. Moreover, exhaust emissions are a trade-off of CI versus SI processes, where soot and NO_x emissions are lower but CO and unburned hydrocarbon emissions are higher than those of direct-injection CI engines. Various researchers have addressed these problems by explaining the effects of use of alternative fuels as pilot fuel, pilot fuel quantity, fuel properties, injection timing, equivalence ratio, intake pressure, temperature and use of EGR [10–24]. Basic natural gas-diesel pilot injection dual fuel technology is currently used in public transportation buses, stationary engines used for power generation, and large-scale ships.

Another common interest in dual-fuel gas engine research is to minimise the pilot fuel injection quantity to reduce diesel fuel dependency while the gaseous fuel is functioning as the major energy source. In these systems, gaseous fuel is fed into the intake air and pilot fuel serves as the source of ignition. Several researchers have focused on this particular application [25–30]. Common observations in these studies include reduced exhaust emissions and improved thermal efficiency over direct injection CI engines [26–28]. Maximization of thermal efficiency is a common goal; however this goal can be achieved by increasing in-cylinder pressure. This high pressure is also the main reason for the increased temperature, which yields to knocking under borderline operating conditions [6–9,12]. This approach is especially beneficial because the fraction of unburned methane rejected in the exhaust gases, a phenomenon known as "methane slip," is reduced [26–27].

Conventional approaches to the use of gaseous fuels in CI engines have strict limitations; thus, more advanced combustion strategies are being investigated, such as Homogeneous Charge Compression Ignition (HCCI) and Reactivity Controlled Compression Ignition (RCCI) [31–36]. HCCI relies of autoignition of in-cylinder mixture, and is suitable for low load operation [31–33]. This strategy provides the foundation of RCCI combustion in terms of mixture preparation and presence of autoignition to a certain extent [34–36]. Currently these two concepts answer the need for low to high load range operation, but can't extend the load range [37].

Dual-fuel operation at high loads has been researched in the laboratory using dual-fuel gas engines with various fuels, including natural gas, and micro pilot fuel injection. Under heavy load conditions, two-stage combustion has been observed as a precursor to knocking with no sign of fluctuations or rapid increase in pressure [38–40]. The thermal efficiency of the engine shows noticeable improvements, with zero smoke emissions. From more recent studies, it is now understood that the end-gas region undergoes autoignition simultaneous with flame propagation; this phenomenon has been named "PREMIER" (PREmixed Mixture Ignition in the End Gas Region) combustion [41–44]. In PREMIER combustion mode, the end-gas region reaches autoignition conditions due to pressure and temperature build-up; simultaneous heat release from two different combustion modes causes more rapid heat release when the engine enters the expansion cycle. While attainable thermal efficiency in this combustion mode is superior to normal operation, the operation range is narrow, limited to the prior-to-knocking operating region. Currently PREMIER combustion is at an early stage of research, and new strategies that can extend its operation range are required in order to provide the tools and methodology required for future practical applications.

In this fundamental study on PREMIER combustion, split pilot fuel injection strategy was applied, and its feasibility as a method to extend the operating range of PREMIER combustion mode is assessed. Delivering the pilot fuel in two parts provided one of the means to control the flame kernels, their size, and the heat release from these sites.

2. Experimental set-up and data evaluation

2.1. Experimental procedure

Schematic diagrams of the performance test and visualization experimental set-ups are shown in Fig. 1. Experiments were conducted in a four-stroke, single-cylinder dual-fuel gas engine. This test engine can also be equipped with an extended piston with an imaging window and other auxiliary equipment for imaging. The engine had a 96-mm bore, a 108-mm stroke, and a compression ratio of 17.0:1 during both performance tests and visualization experiments. The engine is equipped with a shallow dish piston during performance tests. Technical details of the engine are listed in Table 1. Air pressure was stabilised at 101 kPa by a compressor and a surge tank. An air heater stabilised the intake temperature at 313 K, into which natural gas was delivered through a gas injector to prepare a homogeneous intake. This mixture was ignited by the pilot fuel delivered by a diesel fuel injector, equipped with a three-hole nozzle (hole diameter: 0.1 mm). This nozzle is purpose built in order to achieve low injection amounts; therefore its flowrate is restricted, making it unsuitable for 100% diesel fuel operation at medium and high load conditions. Fuel was pressurised by a high-pressure oil pump and sent to the injector through a common rail. The injection pressure was controlled by adjusting the spring inside common rail relief valve. The injection signal was formed from the crank angle (θ) signal obtained each 0.5° of crank angle (°CA), top dead centre (TDC), and cam full revolution signals. The signal duration versus injection amount was calibrated prior to the experiments.

Cylinder pressure was measured with a KISTLER type 6052C pressure transducer connected to a KISTLER type 5011 charge amplifier. In this engine, knocking triggers pressure oscillations at 6.5 kHz, 10.5 kHz and 14 kHz frequencies [41]. Digital filters applied to pressure history are designed based on this criterion. A 4–20 kHz band-pass filter is applied to pressure history for knock analysis. A 6.5 kHz low-pass filter is applied in order to obtain ROHR and performance characteristics. All performance results

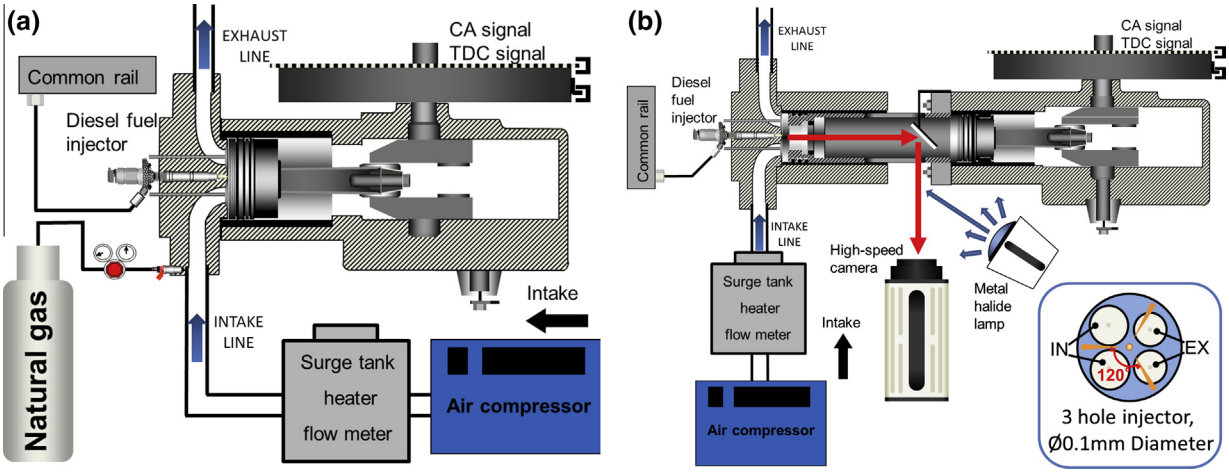

Fig. 1. Experimental setup of (a) performance experiments and (b) visualization.

Table 1
Properties of the test engine.

Bore × Stroke	96 mm × 108 mm
Compression ratio	17:1
Engine speed	1000 rpm
Intake pressure	101 kPa
Equivalence ratio	0.6
Fuel delivery	3 hole, ∅0.1 mm
Injection pressure	40 MPa

were obtained from the pressure history and were calculated over four strokes; thus, the values given are net values– net indicated mean effective pressure (P_{mi}) and net thermal efficiency (η_i). Operating conditions were classified as PREMIER combustion only if more than 50% of the cycles exhibited end-gas autoignition without knocking. The reason behind this will be discussed later. If knocking was observed for at least one cycle, then that operating condition was classified as knocking. Pressure histories and rates of heat release (ROHRs) are presented as averages of 80 consecutive cycles unless indicated as "one cycle" in relevant figures. Knocking operations are represented by a single knocking cycle, having the closest pressure history and ROHR characteristics to the 80-cycle average. All engine performance characteristics derived from the pressure history are presented as averages of 80 consecutive cycles as well. Performance tests were performed without imaging parts, due to their fragile nature under heavy load conditions. The engine has enough clearance to avoid spray and piston surface interaction at given injection timings; therefore flame kernel behaviour is expected to be similar in both performance and visualization experiments.

Experiments are performed at 1000 rpm engine speed, 101 kPa of intake pressure (P_{in}) and an equivalence ratio of 0.6. Injection pressure is fixed at (P_{inj}) for both single and split injection conditions. The main fuel is natural gas, and it is supplied at a rate of 26.7 mg/cycle in performance tests. The diesel fuel injection rate (m_{inj}) was 0.6 mg/cycle in both single and split injection experiments, corresponding to 2% of total energy input. This was decided based on system limitations; the minimum repeatable injection rates were 0.3 mg/cycle with 1.5°CA injection signal duration and 0.6 mg/cycle with 2°CA injection signal duration.

In this work, injection timing refers to the timing of the injection signal. The pilot fuel injector had a delay time of between 1.5 and 2°CA from the rising edge of the injection signal to the delivery of fuel. In single-injection experiments, injection timing (θ_{inj}) was varied from 6° before top dead centre (°BTDC) to 3°BTDC. In split-fuel injection experiments, the first injection timing (θ_1) was varied in the range of 6°BTDC to 3°BTDC and the second injection timing (θ_2) was varied from 3.5°CA after the first injection to θ_2 = 15°ATDC (after top dead centre). Fuel supply strategies are tabulated in Table 2.

2.2. Visualization method

In order search for clues that can explain the results recorded during performance experiments, the engine is equipped with an extended piston of flat top geometry, and a sapphire window with a diameter of 62 mm provides visual access. The difference of combustion chamber geometry, lack of natural gas and difference of combustion chamber materials is expected to alter in-cylinder temperature and pressure; however the results of the visualization experiments are evaluated as clues that explain the effect of second injection timing, and it is expected that the actual sizes of captured flame kernels and the timings of occurrence will show a certain degree of variation between two setups. The cylinder was

Table 2
List of fuel delivery strategies.

	Single			Split				
	θ_{inj}, °BTDC	m_{inj}, mg/cycle	m_{gas}, mg/cycle	θ_1, °BTDC	$m_{inj,1}$, mg/cycle	θ_2, °ATDC	$m_{inj,2}$, mg/cycle	m_{gas}, mg/cycle
Performance	6	0.6, 0.3	26.7	6	0.3	−2.5, −2, −1, 0, 1, 5, 10, 15	0.3	26.7
	5	0.6		5		−1.5, −1, 0, 1, 5, 10, 15		
	4			4		−1.5, 0, 0.5, 1, 2, 3, 4, 5, 10, 15		
	3			3		0.5, 1, 2, 5, 10, 15		
Imaging	6	0.6	0	6	0.3	−1, 0, 5	0.3	0
	5			5		−1, 0, 5		
	4			4		−0.5, 0, 0.5, 5		
	3			3		0.5, 1, 5		

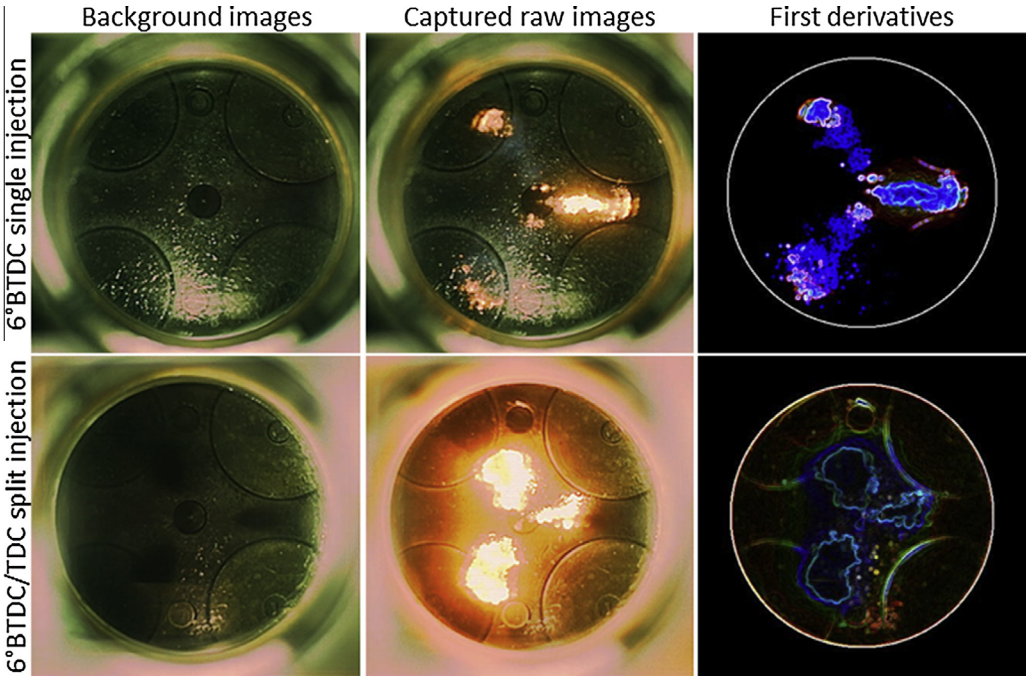

Fig. 2. Examples of background images, in-cylinder images and the first derivatives derived after background subtraction.

illuminated by metal halide lamps through visualization window of the extended piston in order to detect the spray patterns, and the image was reflected to the camera by a mirror. It is observed that the reflections from the metal surfaces of extended piston do not affect the captured image because they appear outside the window extents. In-cylinder images were captured using a high-speed camera at 12 kfps frame rate, which corresponds to two frames per crank angle. The camera was synchronised with the position of the crank through the timer hardware. The first image of the sequence captured at $\theta = 10°$ATDC is used for noise removal in background subtraction method. In addition, blue channels were not sufficiently strong to distinguish with the naked eye and their illumination level is similar to the noise level; thus, first derivatives of the images are given throughout the study in order to distinguish blue flame structures based on their continuity at the edges of the kernel locations. The background images, the original images and the first derivatives after background subtraction are shown in Fig. 2. The white circles in the processed images indicate the boundary of the sapphire window. Additionally, the flame kernels and fuel sprays are hard to distinguish in several images; therefore flame kernels are indicated in yellow circles and spray locations are indicated using small arrows.

3. Engine performance in single injection mode

3.1. Pressure history and rate of heat release

Pressure history and ROHR of normal combustion, PREMIER combustion, and knocking operations with a single injection are presented in Fig. 3. Both pressure history and ROHR of a single typical cycle are given for only $\theta_{inj} = 6°$BTDC to show the indicators of knocking clearly. In normal combustion, autoignition of the pilot fuel creates flame kernels. Combustion of the homogeneous gaseous fuel and air mixture is initiated at these kernels and propagate towards the regions with unburned mixture. When the injection timing is sufficiently advanced, heat release from the propagating flames triggers autoignition in regions with unburned mixture before being consumed by propagating flames. The strength of the end-gas autoignition determines whether the cycle is knocking or PREMIER combustion operation, which is distinguishable by the difference in pressure histories. If a cycle shows a rapid pressure rise with pressure oscillations, then it is a knocking cycle; knocking cycles must be avoided to minimise damage to engine components. However, PREMIER combustion occurs as a precursor to knocking, but the pressure rise is not as steep as in knocking and it does not have any pressure oscillations. Unfortunately, PREMIER combustion showed a very limited operating range, occurring only at $\theta_{inj} = 5°$BTDC under the given operating conditions. Thus, the operation mode spanned from normal operation to knocking combustion when the injection timing advanced 2°CA from $\theta_{inj} = 4°$BTDC to $\theta_{inj} = 6°$BTDC.

3.2. Engine performance and operation stability

Engine performance was evaluated from the indicated mean effective pressure and thermal efficiency. Operation stability is

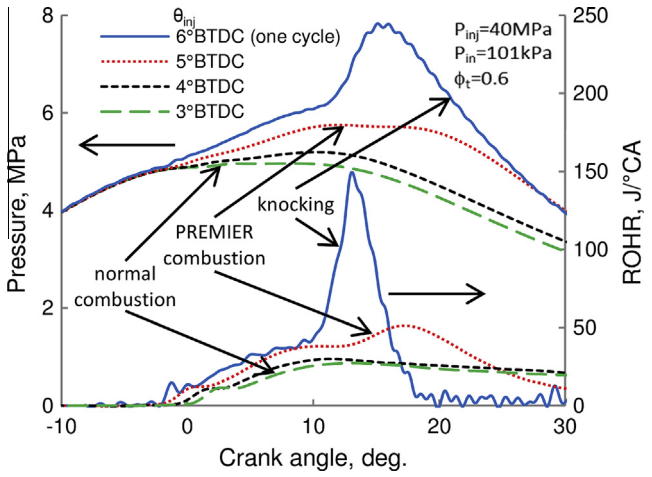

Fig. 3. Typical pressure histories and rates of heat release of normal combustion, PREMIER combustion and knocking operation.

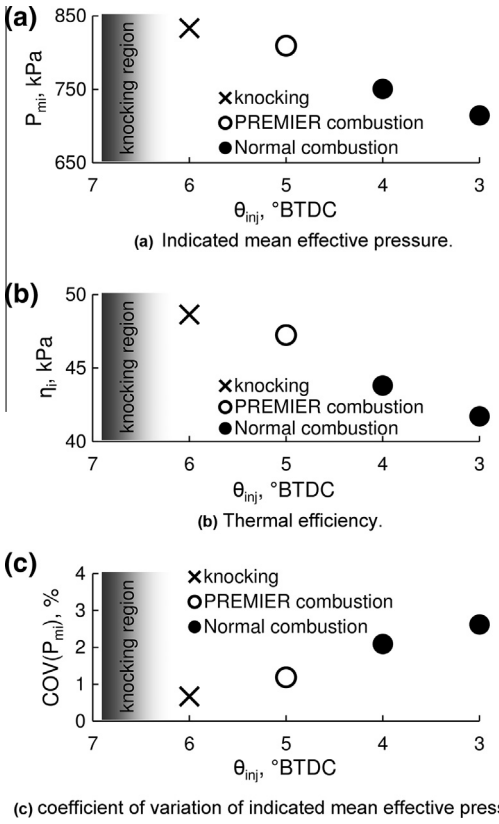

Fig. 4. Engine performance and operation stability with single injection.

explained using the coefficient of variation of the indicated mean effective pressure ($COV(P_{mi})$), given in Fig. 4. The indicated mean effective pressure increased from P_{mi} = 715 kPa to P_{mi} = 833 kPa and thermal efficiency improved from η_i = 41.7% to η_i = 48.6% when the injection timing of θ_{inj} = 3°BTDC was advanced to θ_{inj} = 6°BTDC. Unfortunately, the highest values were recorded during knocking operation. The indicated mean effective pressure and thermal efficiency observed during PREMIER combustion operation at θ_{inj} = 5°BTDC were P_{mi} = 809 kPa and η_i = 47.2%, which are significant increases from P_{mi} = 751 kPa and η_i = 43.8% under normal combustion operation at θ_{inj} = 4°BTDC. This improvement is likely a result of rapid heat release due to autoignition at the end-gas regions. Additionally, the stability of PREMIER combustion operation was superior to that of normal combustion, as shown in the coefficient of variation of the indicated mean effective pressure in Fig. 4(c). Using a single injection strategy, PREMIER combustion was possible only with θ_{inj} = 5°BTDC.

4. Effect of split injection on engine performance and operation range of PREMIER combustion

4.1. Pressure history, rate of heat release, and fraction of PREMIER combustion cycles

Pressure histories and ROHRs of both single and split injection at θ_{inj} = 6°BTDC, θ_{inj} = 5°BTDC, θ_{inj} = 4°BTDC, and θ_{inj} = 3°BTDC are given in Fig. 5(a)–(d), respectively. Due to the many number of operating conditions, several cases resembled or masked the ones given in these figures; thus, some data were omitted. First, these results showed noticeable variation in the ROHR with timing of the second injection. Operations with earlier second injection timings exhibited the most critical variation in both pressure history and ROHR. Fig. 5(a) shows that the overall level of pressure in θ_{inj} = 6°BTDC/2.5°BTDC split injection was lower than the pressure in θ_{inj} = 6°BTDC single injection. In contrast, the overall pressure level was higher in θ_{inj} = 6°BTDC/1°BTDC. The second injection timing of these cases was in the vicinity of the autoignition timing of the first sprays. Similar behaviour was observed in the θ_{inj} = 4°BTDC and θ_{inj} = 3°BTDC cases; thus, it is clear that the sprays of the second injection and the initial stages of flame kernels interact. Furthermore, the effects of split injection were more profound; increased in-cylinder pressure levels were observed over a wider range of second injection timings, as shown in Fig. 5(c) and (d). Delaying the second injection further reduced the in-cylinder pressure and yielded a more gradual heat release profile. In contrast, the lowest incylinder pressure and ROHR were recorded with θ_2 = 5°ATDC during θ_{inj} = 5°BTDC and θ_{inj} = 3°BTDC experiments, an indicator of another critical second injection timing, in which the flame kernels and sprays of the second injection interact in an unusual manner.

The percentages of cycles with end-gas autoignition (ai.) are obtained from 80 cycles at each test condition, and given in Fig. 6. This figure allows discussion of the classification of operating conditions as PREMIER versus normal combustion. Operations may fluctuate between PREMIER and normal combustion operation due to cyclical variations when the intensity of end-gas autoignition is weak; thus, persistence of the occurrence of end-gas autoignition is essential. While the transition between PREMIER and normal combustion has not yet been studied, 50% was selected as a threshold value in this study. The lowest numbers of cycles with end-gas autoignition were observed at single injection in the θ_{inj} = 4°BTDC and θ_{inj} = 3°BTDC cases, both of which had low in-cylinder pressures. When a split injection strategy was applied, both higher cylinder pressures and ROHR were achieved. The higher number of PREMIER combustion cycles in the split-injection experiments was a result of a bigger flame kernel appearing at an earlier timing and allowing heat release to occur earlier. The number of cycles with end-gas autoignition showed a sudden drop in the vicinity of θ_2 = 5°ATDC, which are the lowest numbers in their respective groups, excluding θ_1 = 6°BTDC cases. This suggests that a certain range of second injection timing decelerates heat release substantially and suppresses end-gas autoignition. In fact, the lowest pressure profiles of θ_1 = 5°BTDC and θ_1 = 3°BTDC split-injection experiments were recorded with θ_2 = 5°ATDC, both of which coincided with the lowest percentage of PREMIER combustion cycles.

4.2. Engine performance and operation stability

Engine performance, thermal efficiency, and operation stability of both single and split injection operating conditions are presented in Fig. 7. First, the indicated mean effective pressure and thermal efficiency with first injection timing (θ_1) of 6°BTDC show that it is not possible to suppress knocking if the second injection timing (θ_2) is earlier than TDC. The indicated mean effective pressures did not show much variation until θ_2 = 5°ATDC; however, deterioration was initiated when the second injection timing was later than θ_2 = 5°BTDC. Similar behaviour was observed with θ_1 = 5°BTDC, but deterioration of efficiency began earlier at θ_2 = TDC, reached its minimum value at θ_2 = 5°ATDC, and showed a slight increase thereafter. PREMIER combustion operation was not possible with a single injection at θ_{inj} = 4°BTDC, but could be promoted with a split injection with a second injection timing in the range of 1.5°BTDC–3°ATDC, corresponding to the noticeable increase in the indicated mean effective pressure and thermal efficiency. Suppression of knocking at θ_{inj} = 6°BTDC and promotion of normal combustion to PREMIER combustion at θ_{inj} = 4°BTDC expanded the operation range with PREMIER combustion. The operation ranges of the engine with both single-and

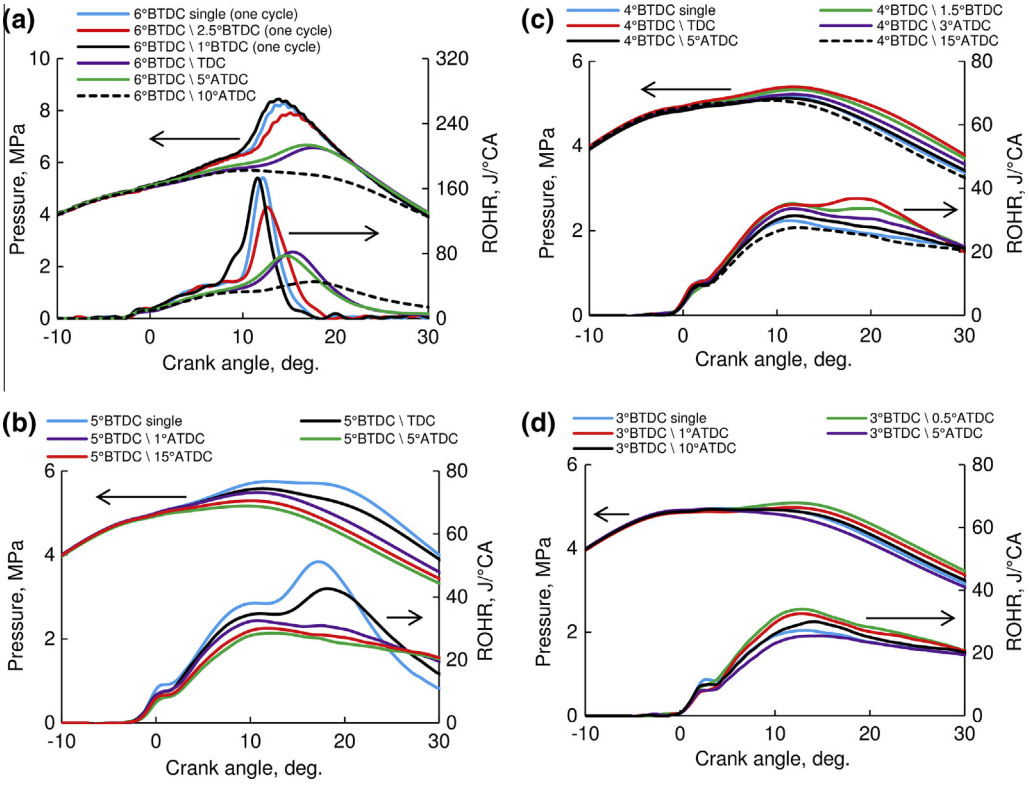

Fig. 5. Pressure histories and rates of heat release with single and split injections at (a) θ_{inj} = 6°BTDC, (b) θ_{inj} = 5°BTDC, (c) θ_{inj} = 4°BTDC, (d) θ_{inj} = 3°BTDC.

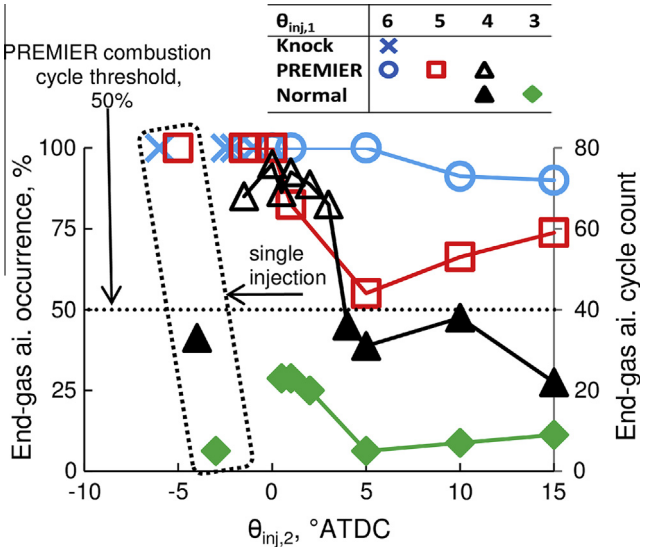

Fig. 6. Percentage of cycles with end-gas autoignition.

split-injection strategies are shown in Fig. 8. While PREMIER combustion was not achievable under any condition at θ_1 = 3°BTDC, split injection still had a positive impact on engine performance. Maximum values of these two performance parameters were recorded with θ_2 = 0.5°ATDC, after which both reached a bottom with a second injection timing of θ_2 = 5°ATDC. The coefficient of variation of the indicated mean effective pressure was smaller when the engine output and combustion efficiency were higher. The coefficient of variation of the indicated mean effective pressure of θ_1 = 6°BTDC cases were lower than COV(P_{mi}) = 1% during both knocking and PREMIER combustion operation until the second injection timing was θ_2 = 5°ATDC. In addition, PREMIER combustion in θ_1 = 4°BTDC operation is in the vicinity of COV(P_{mi}) = 2%.

4.3. Effects of split injection on combustion characteristics

To understand the effect of split injection on PREMIER combustion, it is necessary to discuss the parameters that influence combustion characteristics during this combustion mode. The progression of combustion from pilot fuel injection to the end with heat release can be explained using the ROHR and the second derivative of the ROHR, as shown in Fig. 9 [42]. In this figure, both curves are heavily filtered for easier explanation. After injection, the pilot fuel autoignites at the end of the autoignition delay period and forms flame kernels. The end of the autoignition delay is also detectable as the first significant peak in the second derivative of the ROHR. The duration of autoignition delay is a function of the incylinder temperature and oxygen concentration. Although injection timing does not affect end-gas autoignition timing directly, it affects how early the unburned mixture temperature rises. In the next stage, flame propagation begins from these flame kernels and spreads towards the regions with unburned mixture. Heat release due to flame propagation reaches a detectable rate after the pilot-fuel heat-release peak. At this stage, flame propagation speed and flame kernel size are two important factors that influence the progress of combustion. Flame propagation speed depends on the turbulent burning velocity under the cylinder conditions, such as turbulence intensity, equivalence ratio, unburned gas temperature, and pressure. Flame kernel size does not affect flame propagation speed measurably; however, it determines how early the unburned mixture is consumed. A larger flame kernel ignites a larger volume, which shortens the distance that propagating flames are required to cover. When heat release is sufficiently fast to trigger end-gas autoignition, a third heat release peak appears in the ROHR. This is the indicator of end-gas autoigni-

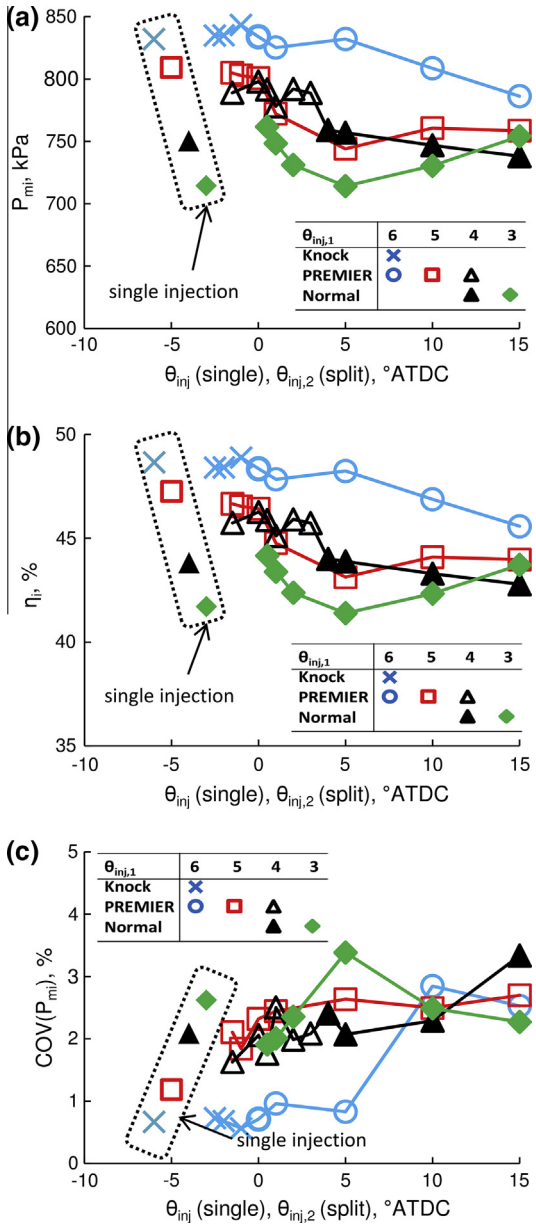

Fig. 7. Effect of split injection on engine performance and operation stability: (a) indicated mean effective pressure, (b) thermal efficiency, and (c) coefficient of variation of indicated mean effective pressure.

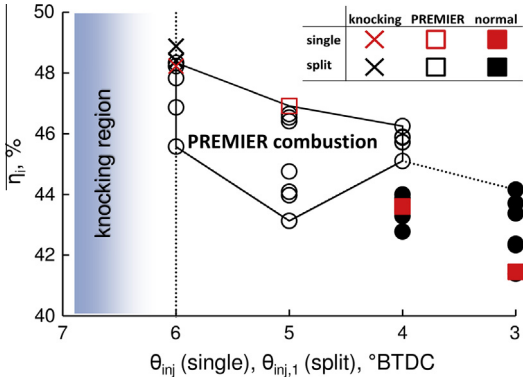

Fig. 8. Operation range of PREMIER combustion with split injection.

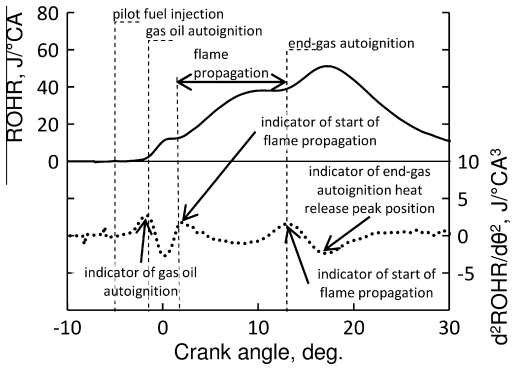

Fig. 9. Typical ROHR and its second derivative in PREMIER combustion as proposed in Ref. [42].

tion in both PREMIER and knocking operations. All of these timings can also be obtained from the second derivative of the ROHR.

Visualization of the effect of split injection on combustion is shown in Fig. 10. Fig. 10(a) shows images of a single injection at θ_{inj} = 5°BTDC. In this condition, the pilot fuel undergoes autoignition instantly and then the flame kernels begin migrating in the injection directions. When a split-injection strategy was applied with injection timings of θ_{inj} = 5°BTDC/1°BTDC, the overall growth rate of the flame kernels became slower, as seen in Fig. 10(b). Additionally, the sizes of the kernels were smaller than those observed with a single injection until θ = 8°ATDC. Flame kernels appeared at the same crank angle in both cases; however, both the location and the size of these kernels differed significantly in the two cases. Kernels of the single injection appeared instantly throughout the injection zones, and their sizes did not change significantly. In contrast, flame kernels for θ_{inj} = 5°BTDC/1°BTDC were small in the initial stage and their growth continued during the next 6.5°CA. Fig. 10(c) shows the behaviour of flame kernel growth in θ_{inj} = 5°-BTDC/5°ATDC, where engine performance and thermal efficiency showed significant deterioration. The flame kernels formed by the first injection reached their full size at a crank angle of 2.5°ATDC and showed no significant sign of growth until 8°ATDC. More detailed sequences displaying the same behaviour are given in Fig. 11 for all split injection cases with second injection timings of θ_2 = 5°ATDC. In these sequences, the flame kernel size was nearly constant until 7°ATDC, followed by inward kernel growth at 7.5°ATDC and kernel growth towards the injection direction at 8°ATDC. This mechanism consumes a fraction of second injection in the vicinity of the injector tip; therefore the second spray does not fully support growth of the flame kernel. Both the resulting flame kernel is smaller and its growth occurs later compared to the rest of the cases with the same first injection timing.

4.4. Suppression of knocking with split injection

To grasp the extent of improvement that can be obtained using a split-injection strategy, a single injection at θ_{inj} = 6°BTDC with m_{inj} = 0.3 mg/cycle injection amount was tested and the results were compared with the results of a single injection θ_{inj} = 6°BTDC with m_{inj} = 0.6 mg/cycle injection amount and split injection in θ_{inj} = 6°BTDC/TDC in Fig. 12. It is possible to suppress knocking in a single-injection strategy by reducing the injection amount; however, this approach has negative impacts on engine output and thermal efficiency. To maximise the efficiency, fast heat release is required without triggering knocking. This goal is achieved using a split-injection strategy, which can control the timing of end-gas autoignition more precisely. After the first injection, the pressure history and ROHR of θ_{inj} = 6°BTDC/TDC and θ_{inj} = 6°BTDC single

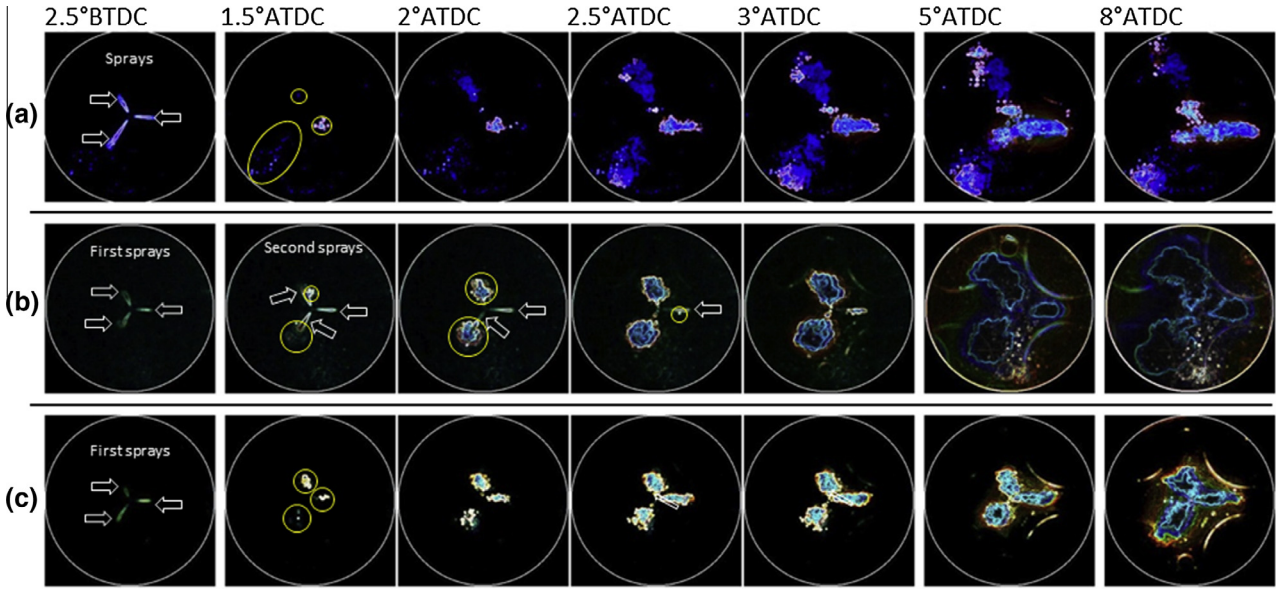

Fig. 10. Flame kernel development at 5°ATDC: (a) θ_{inj} = 5°BTDC single injection, (b) θ_{inj} = 5°BTDC/1°BTDC, and (c) θ_{inj} = 5°BTDC/5°ATDC.

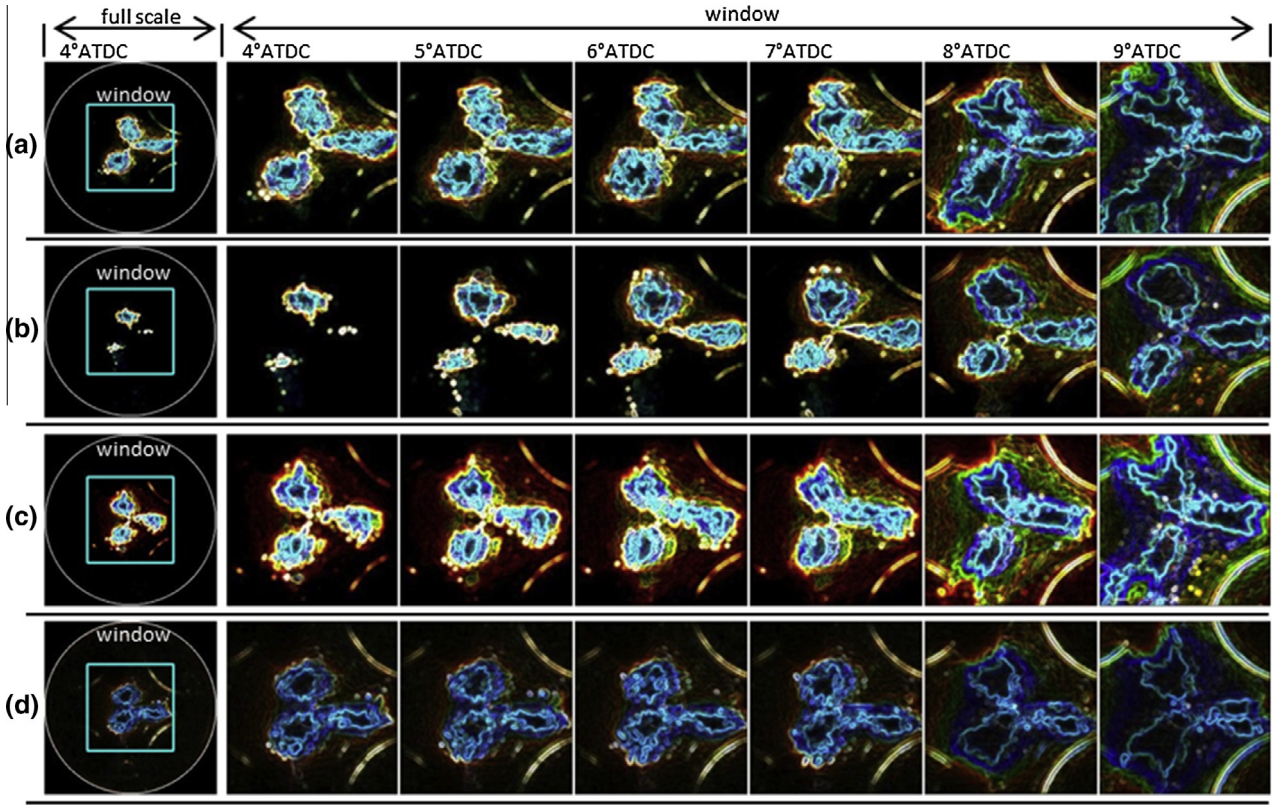

Fig. 11. Closeup view of inward kernel growth with second injection at θ_2 = 5°ATDC. (a) θ_{inj} = 6°BTDC/5°ATDC, (b) θ_{inj} = 5°BTDC/5°ATDC, (c) θ_{inj} = 4°BTDC/5°ATDC and (d) θ_{inj} = 3°BTDC/5°ATDC.

injection with m_{inj} = 0.3 mg/cycle were similar until θ = TDC. Due to the second injection at θ_{inj} = 6°BTDC/TDC, the increases in both in-cylinder pressure and heat release were delayed until θ = 2°ATDC. After this timing, the increases in both in-cylinder pressure and the ROHR at θ_{inj} = 6°BTDC/TDC were faster than those of θ_{inj} = 6°BTDC single injection with m_{inj} = 0.3 mg/cycle, because higher in-cylinder pressure was achieved in the split injection after θ = 8°ATDC. This allows end-gas autoignition to occur earlier, but not so early as to cause knocking. In fact, it was confirmed that heat release in all split-fuel experiments at θ_{inj} = 6°BTDC was faster than the heat release observed in θ_{inj} = 6°BTDC single injection with 0.3 mg/cycle pilot fuel injection.

Kernel development with θ_{inj} = 6°BTDC single injection with 0.6 mg/cycle pilot fuel injection and θ_{inj} = 6°BTDC/TDC are shown in Fig. 13. Images taken at θ_{inj} = 6°BTDC single injection show that flame kernels appeared at 1°ATDC, grew rapidly, and their depth

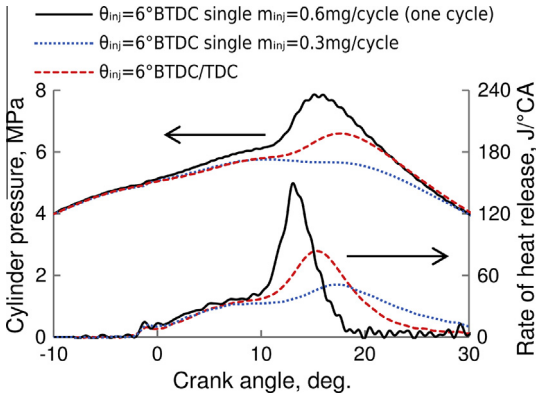

Fig. 12. Comparison of pressure histories and rates of heat release of single and split injection strategies at θ_{inj} = 6°BTDC single injection and θ_{inj} = 6°BTDC/TDC split injection.

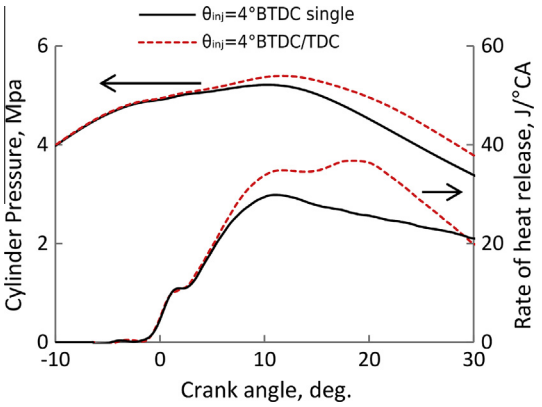

Fig. 14. Comparison of pressure histories and ROHR of single- and split-injection strategies at θ_{inj} = 6°BTDC and θ_{inj} = 4°BTDC.

reached the extent of the sapphire window until 4°ATDC with a single injection. In the image sequence of split-fuel injection, flame kernels appeared at the same time and their sizes were comparable to that of a single injection; however, they grew gradually at a slower rate. These kernels cannot reach as deep as those observed in a single injection until θ = 8°ATDC, but they continued to grow larger. This outcome suggests that reducing the volume of the initial kernels and decelerating their growth delayed the progress of combustion; thus, end-gas autoignition occurred later in the cycle. This mechanism ensures that the expansion rate of the cylinder is sufficiently fast to counteract the pressure rise due to end-gas autoignition.

4.5. Promotion of normal combustion to PREMIER combustion with split injection

Normal combustion can be promoted to PREMIER combustion by accelerating the progress of combustion by split injection (Fig. 14). In a single injection at θ_{inj} = 4°BTDC, the heat release was not fast enough to trigger end-gas autoignition. The ROHR of the flame reached a peak value of about 10°ATDC, after which it slowed down. The behaviour of the split injection case was similar up to a crank angle of 10°ATDC; however, the peak heat release value of flame propagation was higher. In-cylinder pressure rises higher due to faster heat release, which elevates temperature of the unburned mixture. Higher temperature allows faster flame propagation, which advances heat release further and aids the increase of unburned gas mixture temperature. This mechanism satisfies the required conditions for occurrence of autoignition in the end-gas regions. Unfortunately, this mechanism has its limitations. Although split-fuel injection was applied with a first injection timing of θ_1 = 3°BTDC, PREMIER combustion could not be achieved.

Kernel development in θ_{inj} = 4°BTDC single injection and θ_{inj} = 4°BTDC/0.5°ATDC are shown in Fig. 15. The behaviour of the flame kernels in single-injection operation was similar to that of the θ_{inj} = 6°BTDC single injection, but the event was delayed by 2°CA. This time, the second injection was applied with a shorter delay from the first injection. With 3.5°CA timing difference between the first and second injections, the end of delivery of the second injection and the appearance of flame kernels occurred at the same time. As a result, the end of injection coincided with the appearance of flame kernels. According to these sequences, the first flame kernels appeared 1° of crank angle earlier with split injection; however, this may be due to increased luminosity of the kernels on the second sequence, which simplified their visual detection. When the initial locations of flame kernels were compared with those observed in the split-injection sequences of Figs. 10 and 13, the kernels appeared farther from the injector tip in θ_{inj} = 4°BTDC/0.5°ATDC. These two observations indicate that the second spray was not obstructed by the first flames in θ_{inj} = 4°-BTDC/0.5°ATDC; instead, spray penetration potentially increased the rate of kernel growth. The ROHR indicated the initiation of heat release from the pilot fuel between θ = TDC and θ = 1°ATDC. Kernel growth in the θ_{inj} = 4°BTDC/0.5°ATDC split-injection operation was gradual, as was observed for θ_{inj} = 6°BTDC/TDC; however, the flame kernels in θ_{inj} = 4°BTDC/0.5°ATDC grew faster. In fact, kernel growth in the first and second sequences in Fig. 15 were comparable. While kernels of the single injection grew slightly faster

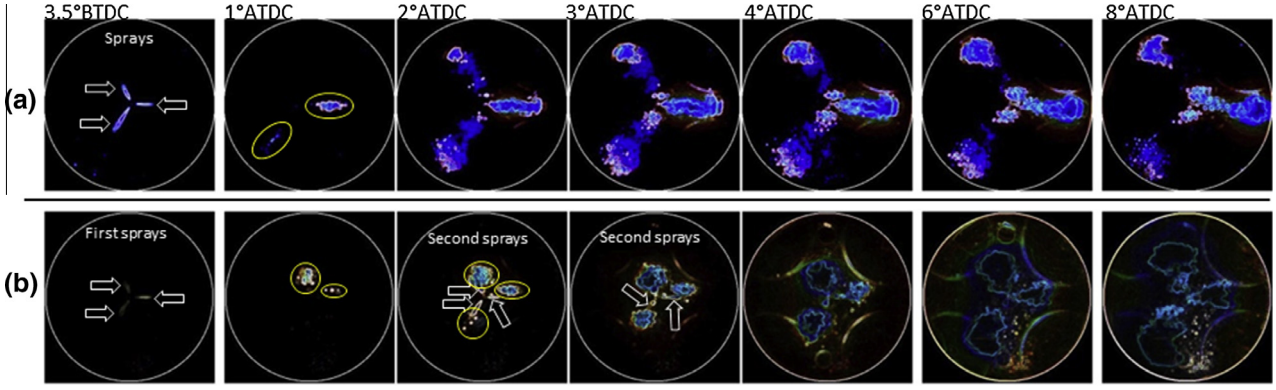

Fig. 13. Visual investigation of suppression of knocking: (a) θ_{inj} = 6°BTDC single injection with m_{inj} = 0.6 mg/cycle and (b) θ_{inj} = 6°BTDC/TDC split injection.

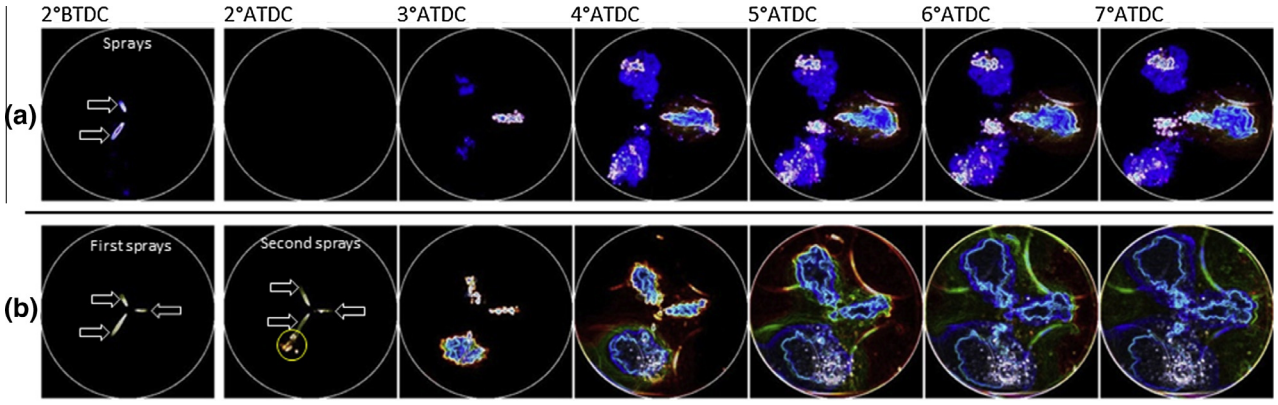

Fig. 15. Visual investigation of promotion of normal combustion to PREMIER combustion: (a) θ_{inj} = 4°BTDC single injection, and (b) θ_{inj} = 4°BTDC/0.5°BTDC.

towards the injection direction, kernels of the split injection grew larger. A similar observation was made for θ_{inj} = 3°BTDC; however, normal combustion could not be upgraded to PREMIER combustion under this operating condition. Instead, engine performance and operation stability improved significantly.

5. Conclusions

In this work, split pilot fuel injection strategy was used in a dual-fuel gas engine in the vicinity of the normal combustion/PREMIER combustion/knocking operation transition to assess the possibility of expanding the operation range of PREMIER combustion. The following conclusions can be made.

(1) Split pilot fuel injection can be used to suppress knocking to obtain PREMIER combustion by delaying the growth of flame kernels and reducing their size. This increases the time required for propagating flames to consume unburned gaseous fuel and air mixture, and retards the overall progress of combustion. The maxima of feasible engine output and thermal efficiency are extended when knocking is suppressed and PREMIER combustion is achieved. The maximum values were similar to those observed during knocking operation.

(2) Split pilot fuel injection can be used to promote normal combustion to PREMIER combustion by widening flame kernels and accelerating their rate of growth. As a result, a larger volume of gaseous fuel and air mixture is consumed earlier, which increases the unburned mixture pressure and temperature faster and earlier. Split injection significantly improves indicated mean effective pressure and thermal efficiency by converting normal combustion to PREMIER combustion. Additionally, it increases the probability of the occurrence of end-gas autoignition when a certain normal combustion operating condition is a precursor to PREMIER combustion.

(3) The range of operating conditions that can be converted to PREMIER combustion by split fuel injection is limited. Heavy knocking or normal combustion with low engine output cannot be converted to PREMIER combustion.

(4) When the end of delivery of the second injection coincides with the appearance of flame kernels, spray penetration supports flame kernel development by increasing both the sizes and growth speeds. When second injection starts before full development of flame kernels, the sprays and kernel initiation zones interact and produce larger flame kernels than is achievable with single injection. When the flame kernels are partially grown during injection, the final size and growth rate of the flame kernels are affected adversely. When the second injection occurs after full growth of the flame kernels formed by the first injection, a fraction of the second spray is consumed in the vicinity of the injector and the kernels grow towards the injector. Consequently, final size of flame kernels is restricted, and their growth is slower, and the fraction consumed around the injector does not provide any input to propagating flames.

(5) The metal engine is expected to have a higher in-cylinder temperature, which changes both spray characteristics and the ignition delay of pilot fuel. This situation dictates that the actual timings and sizes of the flame kernels will possibly differ between two setups, which may raise questions on whether these two cases should be compared directly. On the other hand, the observations made in visualization experiments are in agreement with the performance characteristics obtained in the metal engine. This observation suggests that, the conclusions drawn in visualization experiments can be used for explaining the variations in engine output by estimating the flame kernel behaviour in the metal engine.

References

[1] Rakopoulos DC, Rakopoulos CD, Giakoumis EG. Impact of properties of vegetable oil, bio-diesel, ethanol and n-butanol on the combustion and emissions of turbocharged HDDI diesel engine operating under steady and transient conditions. Fuel 2015;156:1–19.
[2] Rakopoulos DC, Rakopoulos CD, Giakoumis EG, Papagiannakis RG, Kyritsis DC. Influence of properties of various common bio-fuels on the combustion and emission characteristics of high-speed DI (direct injection) diesel engine: vegetable oil, bio-diesel, ethanol, n-butanol, diethyl ether. Energy 2014;73:354–66.
[3] Mustafi NN, Raine RR, Verhelst S. Combustion and emissions characteristics of a dual fuel engine operated on alternative gaseous fuels. Fuel 2013;109:669–78.
[4] Abedin MJ, Imran A, Masjuki HH, Kalam MA, Shahir SA, Varman M, et al. An overview on comparative engine performance and emission characteristics of different techniques involved in diesel engine as dual-fuel engine operation. Renew Sustain Energy Rev 2016;60:306–16.
[5] International Energy Agency. Key world energy statistics; 2015.
[6] Karim GA. A review of combustion processes in the dual fuel engine – the gas diesel engine. Prog Energy Combust Sci 1980;6:277–85.
[7] Karim GA. The dual fuel engine of the compression ignition type - prospects, problems and solutions - a review. SAE technical paper; 1983, 831073.
[8] Karim GA. An examination of some measures for improving the performance of gas fuelled diesel engines at light load. SAE technical paper; 1991, 912366.
[9] Karim GA. Combustion in gas fueled compression: ignition engines of the dual fuel type. J Eng Gas Turbines Power 2003;125(3):827–36.
[10] Wang Z, Zhao Z, Wang D, Tan M, Han Y, Liu Z, et al. Impact of pilot diesel ignition mode on combustion and emissions characteristics of a diesel/natural gas dual fuel heavy-duty engine. Fuel 2016;167:248–56.
[11] Tarabet L, Loubar K, Lounici MS, Khiari K, Belmrabet T, Tazerout M. Experimental investigation of DI diesel engine operating with eucalyptus biodiesel/natural gas under dual fuel mode. Fuel 2014;133:129–38.

[12] Ogawa H, Miyamoto N, Li C, Nakazawa S, Akao K. Smokeless and low NOx combustion in a dual-fuel diesel engine with induced natural gas as the main fuel. Int J Engine Res 2003;4(1):1–9.
[13] Krishnan SR, Biruduganti M, Mo Y, Bell SR, Midkiff KC. Performance and heat release analysis of a pilot ignited natural gas engine. Int J Engine Res 2002;3(3):171–84.
[14] Lounici MS, Loubar K, Tarabet L, Balistrou M, Niculescu DC, Tazerout M. Towards improvement of natural gas-diesel dual fuel mode: an experimental investigation on performance and exhaust emissions. Energy 2014;64:200–11.
[15] Papagiannakis RG, Rakopoulos CD, Hountalas DT, Rakopoulos DC. Emission characteristics of high speed, dual fuel, compression ignition engine operating in a wide range of natural gas/diesel fuel proportions. Fuel 2010;89(7):1397–406.
[16] McTaggart-Cowan GP, Rogak SN, Munshi SR, Hill PG, Bushe WK. The influence of fuel composition on a heavy-duty, natural-gas direct-injection engine. Fuel 2010;89:752–9.
[17] Kakaee AH, Paykani A, Ghajar M. The influence of fuel composition on the combustion and emission characteristics of natural gas fueled engines. Renew Sustain Energy Rev 2014;38:64–78.
[18] Liu J, Zhang X, Wang T, Zhang J, Wang H. Experimental and numerical study of the pollution formation in a diesel/CNG dual fuel engine. Fuel 2015;159:418–29.
[19] Li W, Liu Z, Wang Z. Experimental and theoretical analysis of the combustion process at low loads of a diesel natural gas dual-fuel engine. Energy 2016;94:728–41.
[20] Korakianitis T, Namasivayam AM, Crookes RJ. Diesel and rapeseed methyl ester (RME) pilot fuels for hydrogen and natural gas dual-fuel combustion in compression–ignition engines. Fuel 2011;90(7):2384–95.
[21] Mikulski M, Wierzbicki S. Numerical investigation of the impact of gas composition on the combustion process in a dual-fuel compression-ignition engine. J Nat Gas Sci Eng 2016;31:525–37.
[22] Abagnale C, Cameretti MC, De Simio L, Gambino M, Iannaccone S, Tuccillo R. Numerical simulation and experimental test of dual fuel operated diesel engines. Appl Therm Eng 2014;65(1–2):403–17.
[23] Roy S, Das AK, Banerjee R, Bose PK. A TMI based CNG dual-fuel approach to address the soot–NOx–BSFC trade-off characteristics of a CRDI assisted diesel engine – an EPA perspective. J Nat Gas Sci Eng 2014;20:221–40.
[24] Mousavi SM, Saray SK, Poorghasemi K, Maghbouli A. A numerical investigation on combustion and emission characteristics of a dual fuel engine at part load condition. Fuel 2016;166:309–19.
[25] Singh S, Krishnan SR, Srinivasan KK, Midkiff KC, Bell SR. Effect of pilot injection timing, pilot quantity and intake charge conditions on performance and emissions for an advanced low-pilot-ignited natural gas engine. Int J Engine Res 2004;5(4):329–48.
[26] Micklow GJ, Gong W. Mechanism of hydrocarbon reduction using multiple injection in a natural gas fuelled/micro-pilot diesel ignition engine. Int J Engine Res 2002;3(1):13–21.
[27] May I, Cairns A, Zhao H, Pedrozo V. Reduction of methane slip using premixed micro pilot combustion in a heavy-duty natural gas-diesel engine. SAE technical paper; 2015, 2015-01-1798.
[28] Schlatter S, Schneider B, Wright YM, Boulouchos K. N-heptane micro pilot assisted methane combustion in a Rapid Compression Expansion Machine. Fuel 2016;179:339–52.
[29] Qi Y, Srinivasan KK, Krishnan SR, Yang H, Midkiff KC. Effect of hot exhaust gas recirculation on the performance and emissions of an advanced injection low pilot-ignited natural gas engine. Int J Engine Res 2007;8(3):289–303.
[30] Li W, Liu Z, Wang Z, Dou H, Wang C, Li J. Experimental and theoretical analysis of effects of equivalence ratio on mixture properties, combustion, thermal efficiency and exhaust emissions of a pilot-ignited NG engine at low loads. Fuel 2016;171:125–35.
[31] Thring R. Homogeneous-charge compression-ignition (HCCI) Engines. SAE technical paper; 1989, 892068.
[32] Nobakht AY, Saray RK, Rahimi A. A parametric study on natural gas fueled HCCI combustion engine using a multi-zone combustion model. Fuel 2011;90(4):1508–14.
[33] Manofsky Olesky LK, Middleton RJ, Lavoie GA, Wooldridge MS, Martz JB. On the sensitivity of low temperature combustion to spark assist near flame limit conditions. Fuel 2015;158:11–22.
[34] Kokjohn S, Hanson R, Splitter D, Reitz R. Experiments and modeling of dual-fuel HCCI and PCCI combustion using in-cylinder fuel blending. SAE Int J Eng 2010;2(2):24–39.
[35] Splitter D, Wissink M, DelVescovo D, Reitz R. RCCI engine operation towards 60% thermal efficiency. SAE technical paper; 2013, 2013-01-0279.
[36] Li Y, Jia M, Chang Y, Xie M, Reitz RD. Towards a comprehensive understanding of the influence of fuel properties on the combustion characteristics of a RCCI (reactivity controlled compression ignition) engine. Energy 2016;99:69–82.
[37] Yang Fuyuan, Yao Changsheng, Wang Jinli, Ouyang Minggao. Load expansion of a dieseline compression ignition engine with multi-mode combustion. Fuel 2016;171:5–17.
[38] Tomita E, Harada Y, Kawahara N, Sakane A. Effect of EGR on combustion and exhaust emissions in supercharged dual-fuel natural gas engine ignited with diesel fuel. SAE technical paper; 2009, 2009-01-1832.
[39] Roy MM, Tomita E, Kawahara N, Harada Y, Sakane A. Comparison of performance and emissions of a supercharged dual-fuel engine fueled by hydrogen and hydrogen-containing gaseous fuels. Int J Hydrogen Energy 2011;36(12):7339–52.
[40] Tomita E, Kawahara N, Zheng J. Visualization of auto-ignition of end gas region without knock in a spark-ignition natural gas engine. J Kones Powertrain Transp 2010;17(4):521–7.
[41] Azimov U, Tomita E, Kawahara N, Harada Y. Premixed mixture ignition in the end-gas region (PREMIER) combustion in a natural gas dual-fuel engine: operating range and exhaust emissions. Int J Engine Res 2011;12:484–97.
[42] Azimov U, Tomita E, Kawahara N, Harada Y. Effect of syngas composition on combustion and exhaust emission characteristics in a pilot-ignited dual-fuel engine operated in PREMIER combustion mode. Int J Hydrogen Energy 2011;36(18):11985–96.
[43] Azimov U, Tomita E, Kawahara N. ignition, combustion and exhaust emission characteristics of micro-pilot ignited dual-fuel engine operated under PREMIER combustion mode. SAE technical paper; 2011, 2011-01-1764.
[44] Aksu C, Kawahara N, Tsuboi K, Nanba S, Tomita E, Kondo M. Effect of hydrogen concentration on engine performance, exhaust emissions and operation range of PREMIER combustion in a dual fuel gas engine using methane-hydrogen mixtures. SAE technical paper; 2015, 2015-01-1792.